Bioactive Materials 43 (2025) 406–422

Contents lists available at ScienceDirect

Bioactive Materials

journal homepage: www.keaipublishing.com/en/journals/bioactive-materials

Inhalable and bioactive lipid-nanomedicine based on bergapten for targeted acute lung injury therapy via orchestrating macrophage polarization

Ran Liao [a,1], Zhi-Chao Sun [a,1], Liying Wang [b,d,1], Caihong Xian [b,d], Ran Lin [a], Guifeng Zhuo [e], Haiyan Wang [a], Yifei Fang [b,d], Yuntao Liu [a,*], Rongyuan Yang [a,**], Jun Wu [b,c,***], Zhongde Zhang [a,****]

[a] State Key Laboratory of Traditional Chinese Medicine Syndrome, The Second Affiliated Hospital of Guangzhou University of Chinese Medicine, 55 N, Neihuanxi Road, Guangzhou, 510006, Guangdong, China
[b] Bioscience and Biomedical Engineering Thrust, Systems Hub, The Hong Kong University of Science and Technology (Guangzhou), Nansha, Guangzhou, 511400, Guangdong, China
[c] Division of Life Science, The Hong Kong University of Science and Technology, 999077, Hong Kong SAR, China
[d] School of Biomedical Engineering, Sun Yat-sen University, Shenzhen, 518107, China
[e] Department of The First Clinical College of Medicine, Guangxi University of Chinese Medicine, Nanning, 530000, China

A B S T R A C T

Acute lung injury (ALI) or its more severe form, acute respiratory distress syndrome, is a life-threatening disease closely associated with an imbalance of M1/M2 macrophage polarization. However, current therapeutic strategies for ALI are controversial due to their side effects, restricted administration routes, or poor targeted delivery. The development of herbal medicine has uncovered numerous anti-inflammatory compounds potentially beneficial for ALI therapy. One such compound is the bergapten, a coumarin, which has been isolated from *Ficus simplicissima* Lour. However, it's been used as an anti-cancer drug and it's effects on ALI remain unexplored. The poor solubility and biodistribution of bergapten heavily limit its application. In this timely report, we developed a bioactive and lung-targeting lipid-nanomedicine by integrating bergapten and DPPC liposome, named as Ber-lipo. A comprehensive series of *in vitro* experiments confirmed the anti-inflammatory effects of Ber-lipo and its protective roles in maintaining the homeostasis of macrophage polarization and epithelial–endothelial integrity. In a lipopolysaccharide (LPS)-induced ALI mouse model, Ber-lipo can target inflamed lungs and significantly improve lung edema, tissue injury, and pulmonary function, relieve body weight loss, pulmonary permeability, and proinflammatory status, and especially maintain a balance of M1/M2 macrophage polarization. Furthermore, RNA sequencing analysis showed Ber-lipo's potential in effectively treating inflammatory lung diseases such as pneumonia, inhibiting proinflammatory signals, and altering the transcriptome of M1/M2 macrophages-associated genes in lung tissues. Molecular docking and Western blot analyses validated that Ber-lipo suppressed the activation of the TLR4/MyD88/NF-κB signaling axis responsible for ALI progression. In conclusion, this study demonstrates for the first time that new inhalable nanomedicine (Ber-lipo) can target inflamed lungs and ameliorates ALI by reprogramming macrophage polarization to an anti-inflammatory state via inactivating the TLR4/MyD88/NF-κB pathway, hence providing a promising strategy for enhanced ALI therapy in the clinic.

1. Introduction

Acute lung injury (ALI) or its more severe form, acute respiratory distress syndrome, is a life-threatening clinical condition characterized by features such as an imbalance of M1/M2 macrophage polarization [1–3]. In general, ALI progression can be divided into three stages: uncontrolled inflammation, increased permeability of air-blood barriers, and impairment of pulmonary function and structure [4,5]. With a mortality rate of up to 40%, ALI is one of the deadliest diseases [6,7]. However, there are few effective strategies for ALI therapy in the clinic. Current pharmacological therapies mainly rely on the use of glucocorticoids such as dexamethasone, which often accompany multiple side

Peer review under responsibility of KeAi Communications Co., Ltd.
* Corresponding author.
** Corresponding author.
*** Corresponding authors.
**** Corresponding author.
E-mail addresses: liuyuntao@gzucm.edu.cn (Y. Liu), yangrongyuan@163.com (R. Yang), junwuhkust@ust.hk (J. Wu), doctorzzd99@gzucm.edu.cn (Z. Zhang).
[1] Ran Liao, Zhi-Chao Sun, and Liying Wang contributed equally to this work.

https://doi.org/10.1016/j.bioactmat.2024.09.020
Received 1 August 2024; Received in revised form 7 September 2024; Accepted 17 September 2024

effects including immune system imbalance, coagulation disorders, and osteoporosis [8–10]. Therefore, there is an urgent need to develop novel effective drugs for ALI treatment in the clinic.

As herbal medicine developing, plentiful natural anti-inflammatory compounds have been isolated from herbs, potentially beneficial for ALI therapy [11,12]. Bergapten (5-Methoxypsoralen), a natural coumarin, is mainly found in *Ficus simplicissima* Lour. According to current literature, bergapten possesses significant anti-cancer, anti-inflammatory, and immunomodulatory properties [13–15]. However, the effects of bergapten on treating ALI remain unknown. The insolubility and poor biodistribution of bergapten also present partial obstacles for its clinical application, necessitating the development of a carrier for its delivery.

In recent years, various systems, such as liposomes (Lipo), nanoparticles, and micelles, have shown potential for treating ALI/ARDS due to their good biodistribution, targeting capabilities, or surface modifiability [16–19]. However, there are also concerns about certain carriers because of their toxicity, difficulty in degradation, or low delivery efficiency [20,21]. For instance, chitosan nanoparticles are prone to aggravate lung edema [21]. In the clinic, Lipo system has been approved as a drug carrier by the Food and Drug Administration (FDA). Lipo not only protects drugs from enzymatic degradation before reaching the target sites but also maintains drug stability, reduces drug toxicity, and increases drug solubility for enhanced therapeutic effects [22–24]. In this study, we combined bergapten with Lipo based on dipalmitoyl phosphatidylcholine (DPPC), which is an endogenous saturated phospholipid molecule and a main component of pulmonary surfactants, capable of assisting drug delivery to the lungs [25].

Bergapten was intercalated into the phospholipid bilayers of DPPC Lipo to form a bioactive lipid-nanomedicine (Ber-lipo) for ALI therapy (Scheme 1). Ber-lipo demonstrated good stability, biodistribution, and biocompatibility *in vitro* and *in vivo*. Additionally, Ber-lipo ameliorated multiple ALI phenotypes in mice, such as lung edema, proinflammatory status, lung damage, pulmonary dysfunction, and lung permeability. Further, Ber-lipo maintained the homeostasis of macrophage polarization by reducing proinflammatory M1-type and increasing anti-inflammatory M2-type, which can facilitate a series of ALI phenotypes [26]. Mechanistically, Ber-lipo suppressed the activation of the TLR4/MyD88/NF-κB signaling pathway. Taken together, this study is the first to demonstrate that lung-targeted Ber-lipo alleviates ALI via

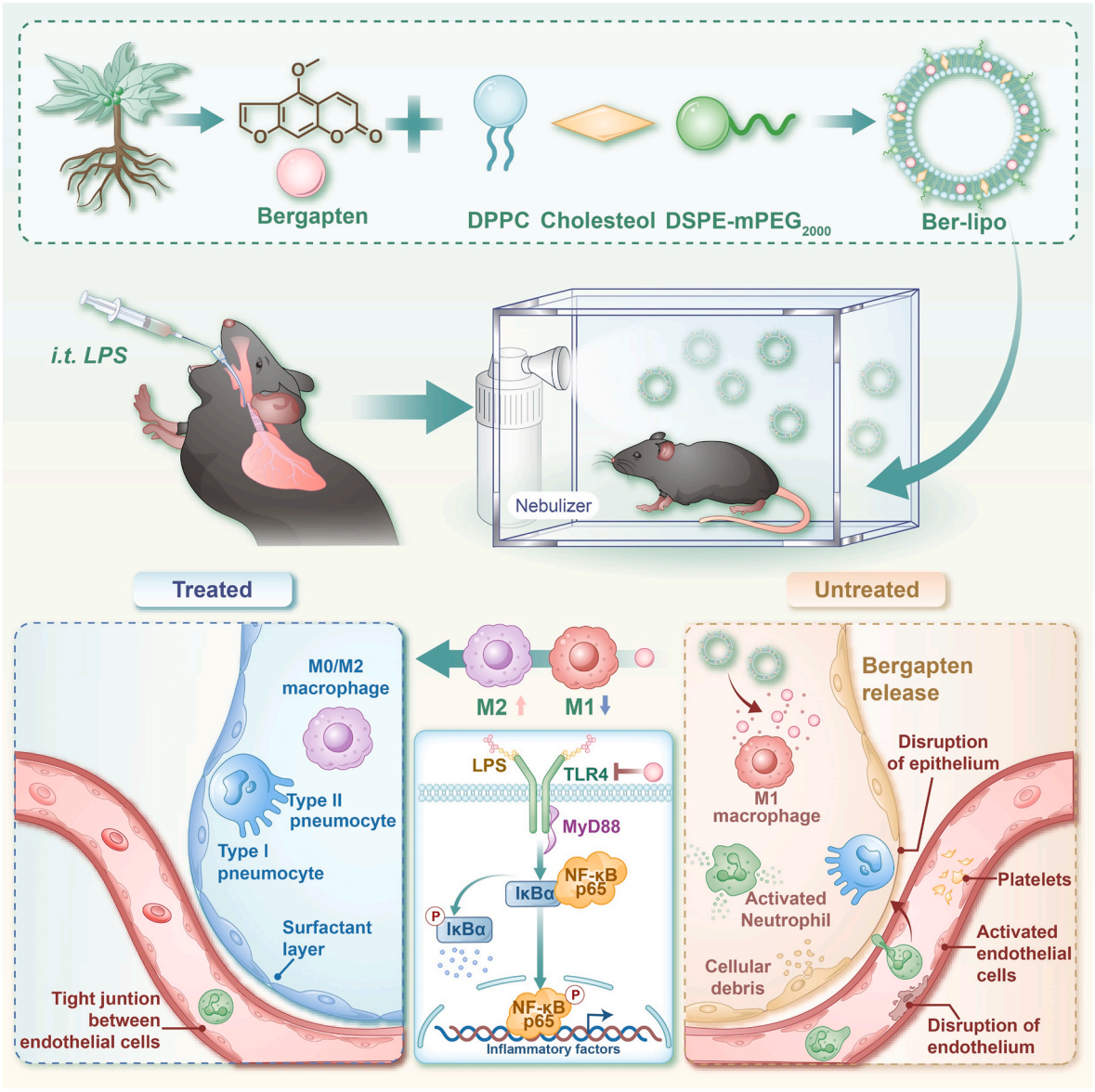

Scheme 1. Development of bioactive and lung-targeted Ber-lipo for enhanced murine ALI therapy through maintaining the homeostasis of macrophage polarization via inhibiting the activation of the TLR4/MyD88/NF-κB signaling pathway.

TLR4/MyD88/NF-κB-mediated macrophage polarization, hence providing a promising candidate strategy for ALI treatment in the clinic.

2. Results and discussion

2.1. Synthesis and characterization of ber-lipo

Bergapten, isolated from *Ficus simplicissima* Lour, has demonstrated anti-cancer and anti-inflammatory properties but suffers from poor solubility in water. In order to address this limitation, a lipid-nanomedicine based on bergapten (referred to as Ber-lipo) was developed, in which the drug was intercalated into lung-targeted DPPC Lipo [27,28]. Transmission electron microscopy (TEM) analysis revealed that both Lipo and Ber-lipo exhibited a uniform spherical morphology with a diameter of approximately 115 nm (Fig. 1A). To confirm this observation, dynamic light scattering was employed to determine their size distributions. Consistent with the TEM results, the average particle size of Lipo and Ber-lipo were measured to be 111.2 nm and 116.1 nm, respectively (Fig. 1B). Subsequently, electrophoretic light scattering was utilized to measure the zeta potentials of these formulations when diluted in water at room temperature. As depicted in Fig. 1C, the zeta potentials of Lipo and Ber-lipo were found to be −9 mV and −7 mV, respectively, indicating that bergapten had an opposite charge to Lipo, which was favorable for their binding. To assess the stability of Lipo and Ber-lipo, their size distributions were monitored over a period of 7 d, and it was found that they consistently fluctuated around 110 nm (Fig. 1D). Similarly, their polydispersity index ranged from 0.15 to 0.22 over the consecutive 7 d (Fig. 1E). Thus, it was concluded that the nanosized Ber-lipo formulations remained stable in water for at least 7 d.

Further, Lipo's biodistribution was evaluated in RAW264.7 cells with or without LPS stimulation. Hydrophobic compound Dil (40726ES10, Yeasen, Shanghai, China) was utilized to label Lipo (Dil@lipo) by the same fabrication process as that of Ber-lipo. Cells were incubated with free Dil or Dil@lipo for 4 h. As shown in Fig. 1F, free Dil (red) only existed in cytoplasm of partial cells where its distributions were uneven; differently, Dil@lipo entered into all cells' cytoplasm with very uniform distributions; LPS stimulation couldn't change their biodistribution pattern. Likewise, bergapten is also a hydrophobic compound with poor biodistribution, which may be overcome by integrated in Lipo (Ber-lipo).

Drug delivery efficiency of lung tissues has been essential for ALI treatment. To further assess the lung-targeting property of Ber-lipo in ALI mice, hydrophobic Dir, a near infrared fluorescent dye used for *in vivo* imaging system (IVIS; AniView Kirin, BLT, China) [29], was intercalated in Lipo (Dir@lipo) by the same way as that of bergapten. The distributions of Dir and Dir@lipo in main organs were observed with IVIS at 1 h, 4 h, and 24 h after intraperitoneal injection of them (Fig. 1G). Results showed that after 1 h, the distribution of Dir@lipo in all organs was obviously more than that of free Dir, where fluorescence mainly existed in livers and lungs probably due to liver metabolism and lung-targeting (Fig. 1H), respectively [30]. With time going, Dir@lipo accumulated more and more in lungs rather than in livers, exhibiting an incremental increase in the fluorescent ratio of lung to liver (Fig. 1I-K). Besides, significantly stronger fluorescent intensity was found in the blood of the Dir@lipo group as compared to the free Dir treatment (Fig. 1L), indicating that Dir@lipo had good stability, distribution, and biocompatibility in blood.

For drug delivery systems targeting lung, there are many affecting factors, such as surface charge, size, interaction with pulmonary surfactants, responsiveness to the microenvironment, and surface modifications [21]. Firstly, lung-targeting Lipo can be categorized into three types according to various surface charges determined by the lipid head groups: a) Neutral Lipo can be internalized by most lung cells; b) Anionic Lipo with negative potentials are prone to be phagocyted by alveolar macrophages; c) Cationic Lipo possess positive potentials and are preferentially taken up by infiltrated neutrophils in the lung [31,32]. Besides, it seems nanocarriers with positive potential are more beneficial for lung accumulation such as DOTAP Lipo, but they are more toxic. This toxicity can be reduced by incorporating DPPC, a strategy that balances efficacy and safety in lung-targeted drug delivery [21,33,34].

Secondly, an increase in nanoparticle size tends to enhance the accumulation of drugs in the lungs [21]. However, for pharmaceutical applications, particularly those involving parenteral administration, nanoparticles of smaller size (≤100 nm) are more advantageous [32]. The size of Lipo can range from 20 to approximately 1000 nm. To strike a balance between lung accumulation and pharmacological effects, the size of Lipo can be flexibly adjusted through various techniques, such as sonication, extrusion, homogenization, and microfluidic methods [32]. Thus, optimizing the size of Ber-lipo is crucial for augmenting it's therapeutic effects on ALI in future studies.

Thirdly, Pulmonary surfactants especially phosphatidylcholine (PC; e.g., DPPC and DOPC) can be utilized in Lipo to facilitate drug delivery to the alveoli [21,28]. Finally, passive targeting delivery can be realized through microenvironment (ROS, pH, and inflammation)-responsive nanocarriers due to enhanced lung permeability during ALI. On the contrary, surface modification (e.g., antibodies) can assist drugs in active targeting specific cells in lung [21]. Based on these strategies, it is of great significance to optimize Ber-lipo's lung targeting property in the future for improving its therapeutic effects.

Altogether, this finding established a reliable method for delivering therapeutic agents such as bergapten to the inflamed lungs by using DPPC Lipo as a carrier, which is very important for ALI targeted therapy.

2.2. Good biocompatibility of ber-lipo in vitro and in vivo

To evaluate the biocompatibility of Ber-lipo *in vitro*, RAW264.7 and human umbilical vein endothelial cells (HUVECs) were utilized. The cells were treated with Lipo, bergapten, or Ber-lipo for 12 or 24 h. Subsequently, CCK-8, live/dead staining, and cytoskeleton staining were performed to evaluate the cytotoxicity of the drugs. The results from the CCK-8 assay showed that cell viability in the bergapten (2.5−40 μM) and Ber-lipo (2.5−40 μM) groups was similar to that of the control in both RAW264.7 and HUVECs (Fig. 2A & B). However, we also found 80 μM of bergapten but not Ber-lipo cause 24% of HUVECs to die (Fig. 2B), indicating Lipo obviously mitigated bergapten's cytotoxicity. As reported, bioactive molecules, such as bergapten, are potential drugs, but they are also potent toxins, which can be weakened by some nanoscale delivery systems (namely nanoantidotes) [35,36]. Thus, Lipo might be a potential nanoantidote as a detoxification delivery system for those toxic drugs.

Based on aforementioned results, 40 μM bergapten and 40 μM Ber-lipo were used for live/dead and cytoskeleton staining. The live/dead staining showed that there were almost 100% live cells (Calcein AM, green) and very few dead cells (propidium iodide, red), and there was no disruption of the cytoskeleton (Phalloidin, green) in HUVECs (Fig. 2C & D), demonstrating good biocompatibility of Ber-lipo *in vitro*.

For the assessment of the drugs' biocompatibility *in vivo*, a hemolysis assay and haematoxylin-eosin (HE) staining were performed. Hemolysis is a crucial indicator to assess the hemocompatibility of drugs, as it is related to the occurrence and progression of numerous diseases [37]. The hemolysis ratio of different concentrations of bergapten and Ber-lipo (5–80 μM) was evaluated, and it was observed that the drug treatment and negative control groups exhibited very light color (indicating low hemolysis) as opposed to the deep color (indicating high hemolysis) in the positive control. The hemolysis ratio was quantified using a microplate reader, and the values were lower than 5% in the drug intervention groups (Fig. 2E), indicating little hemolysis. Furthermore, to assess the safety of the drugs on main organs in LPS-induced ALI mice, HE staining was employed. The results showed no significant histopathological changes in the heart, kidney, liver, and spleen tissues among all groups (Fig. 2F). In conclusion, the good biocompatibility of Ber-lipo was successfully confirmed *in vivo*.

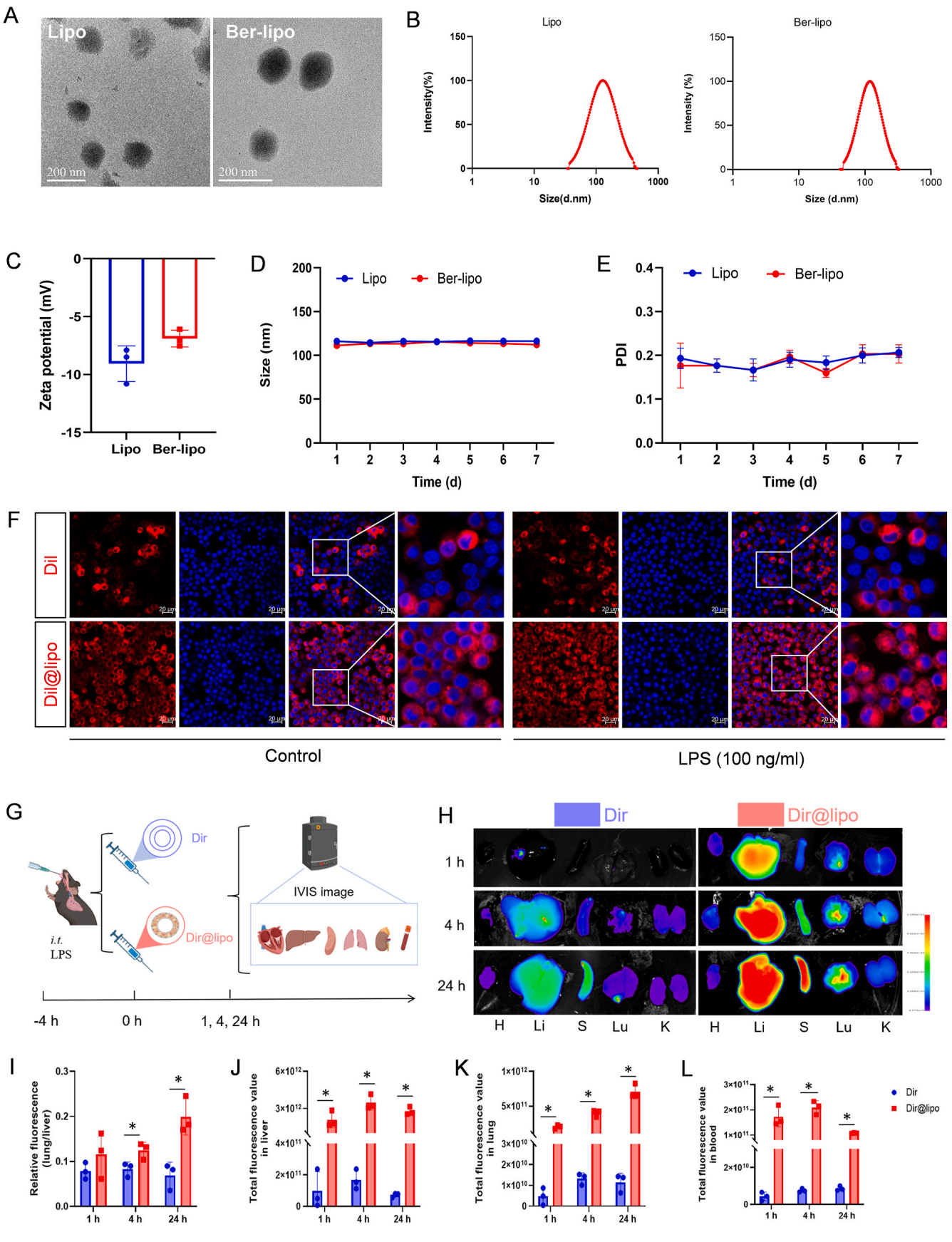

(caption on next page)

Fig. 1. The characterization of Ber-lipo. (A) Morphology of the Lipo and Ber-lipo visualized using TEM. Scale bar, 200 nm. (B) Size distributions of the Lipo and Ber-lipo analyzed by dynamic light scattering method. (C) Surface zeta potentials of the Lipo and Ber-lipo diluted in water at room temperature tested by electrophoretic light scattering method. (D) Size stability of the Lipo and Ber-lipo when stored in water over a period of 7 d. (E) Polydispersity index of the Lipo and Ber-lipo in water within consecutive 7 d. (F) The biodistribution of Dil/Dil@lipo in RAW264.7 cells with or without LPS stimulation imaged by confocal microscope (LSM710, Zeiss, Germany). Scale bar, 20 μm. (G) Schematic illustration of the biodistribution of Dir/Dir@lipo in ALI mice observed under IVIS. (H–L): (H) *In vivo* biodistribution of Dir@lipo and Dir in main organs at different time periods after intraperitoneal injection of them via IVIS imaging. H, heart. Li, liver. S, spleen. Lu, lung. K, kidney. (I) Statistical analysis of fluorescent intensity ratio of lung to liver for each group (n = 3). (J–L) Statistical analysis of fluorescence intensity in the livers, lungs, and blood (n = 3). $^{*}P < 0.05$.

The biosafety of Ber-lipo can largely be attributed to its liposomal carrier composition. Lipo represents the earliest generation of nanomedicine delivery system and has been applied in medicine for over 50 years [32]. As a versatile nanocarrier, it can encapsulate and deliver a variety of medications, including hydrophilic, hydrophobic, and amphiphilic drugs, to treat various diseases. Hitherto, plenty of liposomal formulations have been approved for clinical use [32]. For instance, Amikacin Liposome Inhalation Suspension (ALIS) is utilized for lung infections, including ALI [28]. Thus, in this study, Lipo was selected as the carrier for delivering bergapten. The main component of Ber-lipo is DPPC, a pulmonary surfactant. DPPC not only assists bergapten to target lung but also can replenish the intrinsic compounds of the impaired pulmonary surfactants in inflamed lungs [20]. Given the benefits of DPPC, it is also incorporated into many cationic liposomal formulations to reduce their toxicity [33]. Collectively, these clinical advantages and biosafety of Lipo make it as first choice to deliver bergapten for ALI therapy.

2.3. Ber-lipo's effects on maintaining the homeostasis of macrophage polarization in vitro

The balance of M1/M2 macrophage polarization plays a crucial role in the entire progression of ALI, including the regulation of inflammatory status, rehabilitation of lung injury, and pulmonary barrier repair [26]. In the acute phase of ALI, proinflammatory M1 macrophages significantly increase and release inflammatory factors such as TNF-α, IL-6, and IL-1β, leading to uncontrolled inflammation, lung damage, and barrier disruption. In the late phase of ALI, anti-inflammatory M2 macrophages increase and produce anti-inflammatory cytokines (e.g., CCL22 and CCL24) to aid in lung recovery [38]. Therefore, maintaining the homeostasis of M1/M2 macrophage polarization has been considered a promising strategy for treating ALI or other related diseases [39,40].

To evaluate the effects of Ber-lipo on M1/M2 macrophage polarization, immunofluorescent staining, Western blot, flow cytometry, and qRT-PCR were performed to assess the expression of M1- and M2-associated markers in RAW264.7 cells. In the immunofluorescence analysis, an increase in CD86 expression (indicative of M1 macrophage, red) was observed post-LPS stimulation, which decreased following treatment with bergapten or Ber-lipo. In contrast, CD163 expression (indicative of M2 macrophage, red) demonstrated an opposite pattern (Fig. 3A). Flow cytometry analysis further corroborated these findings, revealing a decrease in the proportion of $CD86^{+}$ M1 macrophages following drug treatments. Specifically, the proportion of $CD86^{+}$ cells was reduced to 4.03% with bergapten and 3.22% with Ber-lipo, both markedly lower than the 8.11% observed in the model group. Conversely, the proportion of $CD163^{+}$ M2 macrophages was 57.8% and 73.1% in the bergapten and Ber-lipo treatment groups, respectively, significantly higher than in the model group (25.9%) (Fig. 3B & Fig. S1).

Furthermore, the protein and mRNA expressions of M1/M2-associated genes were assessed using Western blot and qRT-PCR, respectively. As shown in Fig. 3C & D, the results showed that the protein expression of CD86 was significantly upregulated in the model group compared to the control, and this was reversed by the addition of the drugs, with Ber-lipo showing greater efficacy than bergapten. Conversely, the protein expression pattern of CD163 was opposite to that of CD86. Additionally, the mRNA expressions of M1 markers (CD86 and iNOS) and their released TNF-α, IL-6, and IL-1β were elevated by LPS stimulation and then declined following treatments with bergapten or Ber-lipo. On the contrary, the transcriptional levels of M2-associated genes, CD206, CCL22, and CCL24, were found to be downregulated in the model group when compared to the control group, which was significantly rescued by Ber-lipo intervention (Fig. 3E-L).

In summary, Ber-lipo effectively maintained the balance of macrophage polarization by reducing M1 and increasing M2 for the transition from a proinflammatory to an anti-inflammatory state in the LPS-induced microenvironment *in vitro*. This suggests that Ber-lipo may have beneficial effects against inflammatory diseases or tissue injury.

2.4. Protective effects of ber-lipo on epithelial and endothelial integrity in vitro

In addition to the imbalance of macrophage polarization and uncontrolled inflammation, ALI is often initiated or aggravated by air-blood barrier damage [41,42]. Maintaining the lung barrier is an effective and important strategy for ALI treatment. Zonula occludens-1 (ZO-1), a peripheral membrane protein of tight junctions essential for epithelial and endothelial integrity, is localized at the site of adhesion junctions during early formation [43–45]. In this study, we utilized HUVEC and MLE-12 cells to evaluate the protective effects of Ber-lipo on endothelial and epithelial integrity by analyzing ZO-1 expression patterns, respectively.

Immunofluorescent staining was conducted initially. The results in Fig. 4A showed that ZO-1 protein (red) was significantly reduced, ruptured, or irregularly arranged in the model group compared to the control in both MLE-12 and HUVEC cells, indicating enhanced permeability. Conversely, ZO-1 protein sealed intercellular spaces in the bergapten and Ber-lipo treatment groups, indicating the restoration of integrity. To accurately quantify ZO-1 expression, Western blot analysis was performed in MLE-12 and HUVEC cells exposed to LPS stimulation. From Fig. 4B, it was observed that ZO-1 expression was decreased in the model group compared to the control in both cell types, and this reduction was then reversed by the addition of the drugs, with Ber-lipo showing greater efficacy compared to bergapten. These findings revealed that Ber-lipo effectively repaired the disruption of epithelial and endothelial barriers *in vitro*.

2.5. Protective effects of ber-lipo on LPS-induced ALI in mice

After confirming the effects of Ber-lipo on maintaining the homeostasis of M1/M2 macrophages, inhibiting inflammation, and protecting epithelial and endothelial integrity *in vitro*, we proceeded to verify Ber-lipo's therapeutic effects on an ALI model. ALI mice were established by intratracheal injection of LPS (5 mg/kg) and then treated by inhalation of bergapten and Ber-lipo for 3 d (Fig. 5A). Multiple ALI phenotypes were tested, such as lung histopathology, body weight loss, lung edema, inflammation, and lung permeability.

In the histopathological analysis (Fig. 5B), it was observed that the model group exhibited noticeable inflammatory cell infiltration, disruption of alveolar structure, and bloody exudation, which were significantly alleviated by inhaled bergapten and Ber-lipo. Pathological scores based on HE staining showed that Ber-lipo significantly ameliorated lung injury in LPS-induced ALI mice (Fig. 5C). Additionally, body weight loss, a key index of numerous acute inflammatory diseases

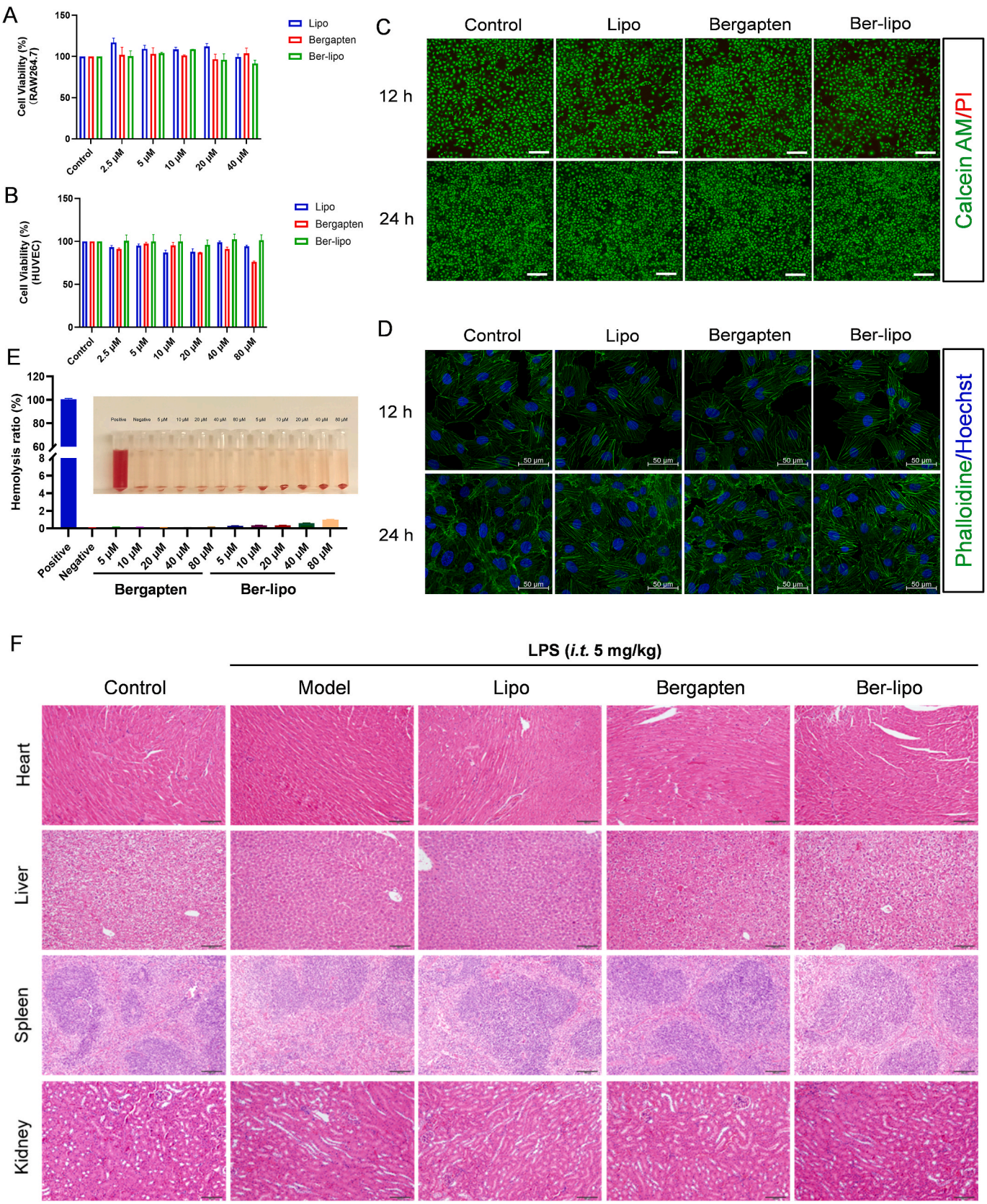

Fig. 2. Good biocompatibility of Ber-lipo *in vitro* and *in vivo*. (A, B) CCK-8 assays in RAW264.7 and HUVEC cells, respectively (n = 3). (C) Live/dead cell staining in HUVEC. Green, Calcein AM staining for live cells. Red, propidium iodide staining for dead cells. Images were taken at 100 × magnification. Scale bar, 250 μm. (D) Cell skeleton staining in HUVEC. Images were captured using 40 × oil lens of confocal microscope (LSM710, Zeiss, Germany). Green, FITC phalloidine. Blue, DAPI. Scale bar, 50 μm. (E) Hemolysis ratio assays of Ber-lipo (n = 3). (F) Histopathological evaluation of heart, liver, spleen, and kidney of LPS-induced ALI mice using HE staining.

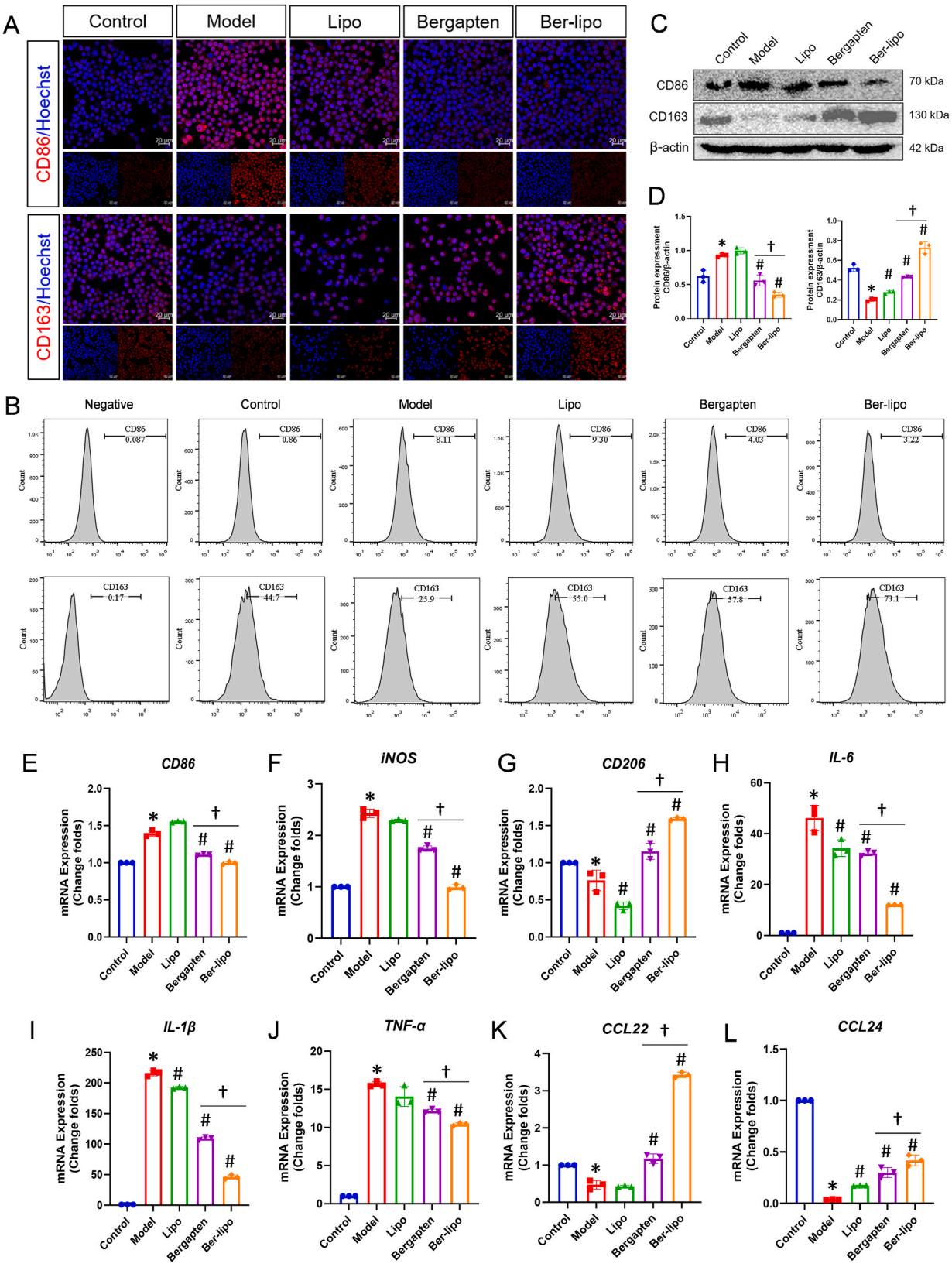

Fig. 3. Ber-lipo's effects on maintaining balance between M1 and M2 macrophage polarization *in vitro*. (A) The distribution of CD86-marked M1 and CD163-indicated M2 in RAW264.7 cells by immunofluorescent staining (red). Images were captured using 40 × oil immersion lens of confocal microscope. Scale bar, 20 μm. (B) The proportion of $CD86^{+}$ M1 and $CD163^{+}$ M2 in RAW264.7 cells by flow cytometry. (C) Protein expression of CD86 and CD163 in RAW264.7 cells by Western blot. (D) Quantification of protein bands by imageJ software (n = 3). (E–L) The normalized mRNA expressions of CD86, iNOS, CD206, IL-6, IL-1β, TNF-α, CCL22, and CCL24 using qRT-PCR. Internal control, α-Tubulin. M1 phenotypic markers: CD86, iNOS, IL-6, IL-1β, and TNF-α. M2 phenotypic markers: CD163, CD206, CCL22, and CCL24. Model, RAW264.7 cells challenged by 100 ng/ml LPS. *$P < 0.05$ vs Control. #$P < 0.05$ vs Model. †$P < 0.05$.

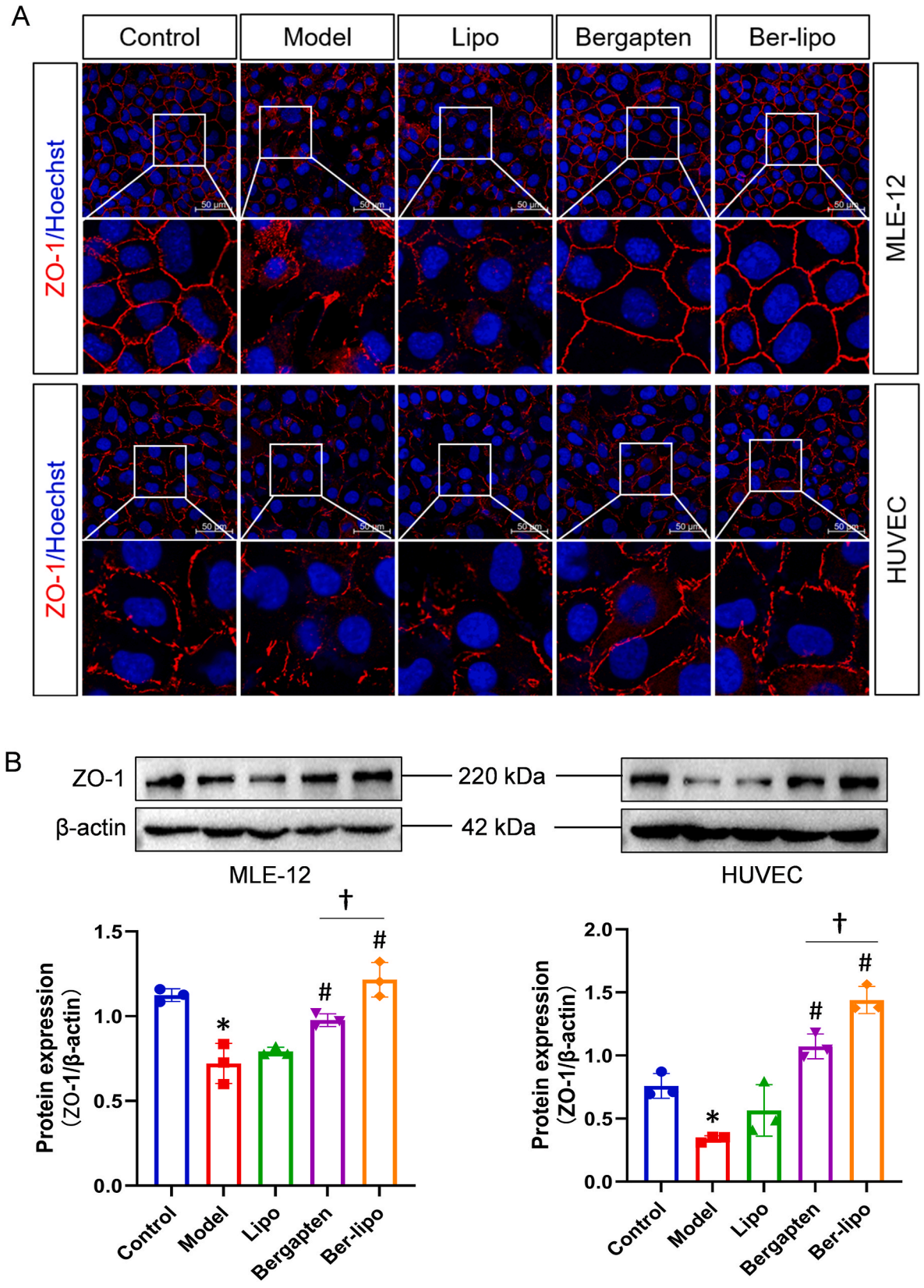

Fig. 4. Protective effects of Ber-lipo on epithelial and endothelial integrity *in vitro*. (A) The expression pattern of ZO-1 protein by immunofluorescent staining in MLE-12 and HUVEC cells, respectively. Images were captured using 40 × oil lens of confocal microscope. Scale bar, 50 μm. (B) The protein expression of tight junction factor (ZO-1) in MLE-12 and HUVEC cells by Western blot. The expression levels were calculated by ImageJ software (n = 3). Internal control, β-actin. $^{*}P < 0.05$ vs Control. $^{\#}P < 0.05$ vs Model. $^{\dagger}P < 0.05$.

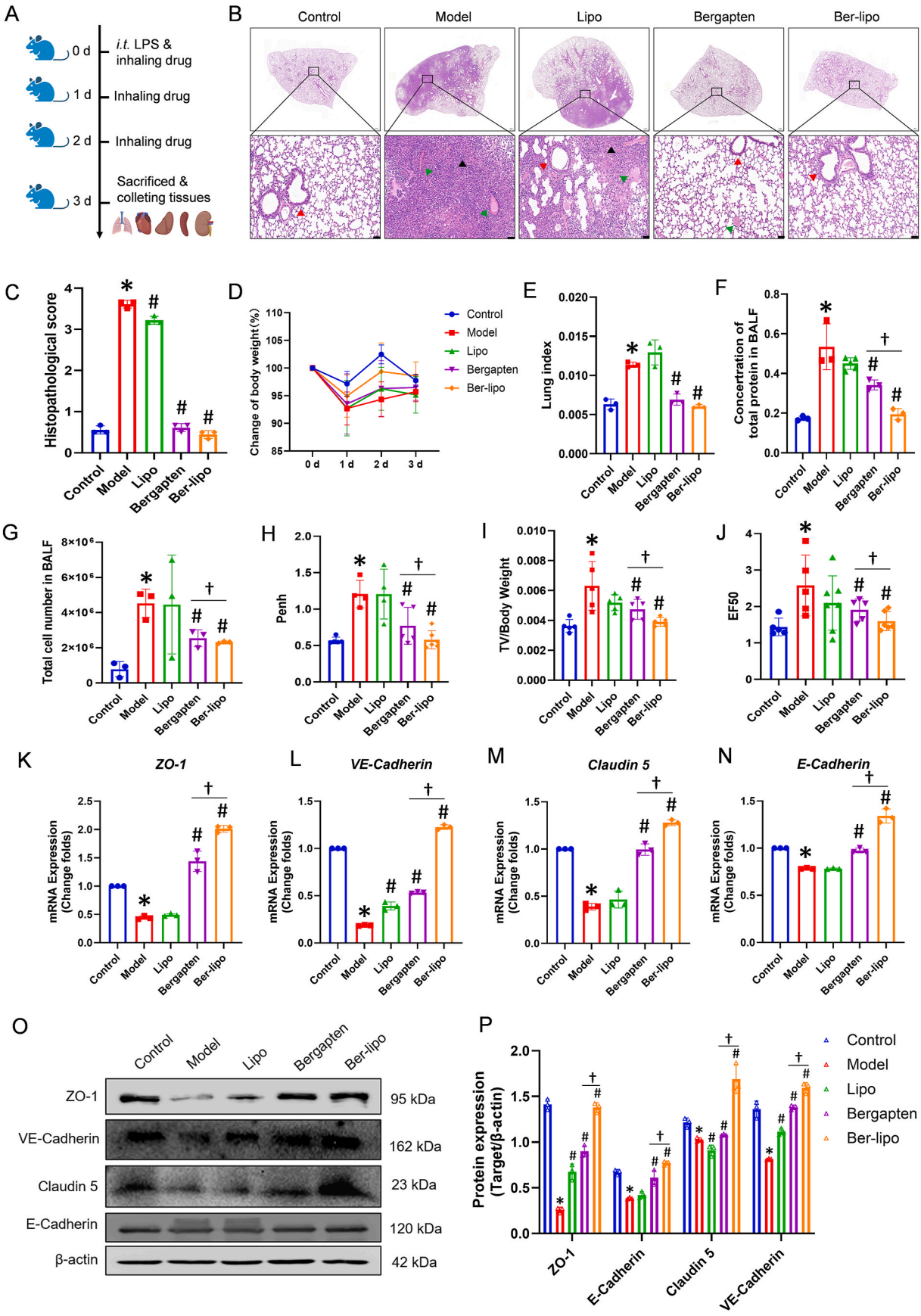

Fig. 5. Ber-lipo relieved LPS-induced ALI *in vivo*. (A) Schematic illustrating of animal experimental design. (B) Histopathology of lung tissues by H&E staining. Scale bar, 50 μm. Black arrows, inflammatory cell infiltration. Red arrows, disruption of alveolar structure. green arrows, bloody exudation. (C) Pathological scores of HE staining results (n = 3). (D) Changes of murine body weight loss among all groups for 3 d (n = 3). (E) Lung index of ALI mice (n = 3). (F, G) Total protein content

and cell number in BALF (n = 3). (H–J) Pulmonary function of mice (n = 3). (K–N) The normalized mRNA expression of tight junction factors, ZO-1, VE-Cadherin, Claudin 5, and E-Cadherin, by qRT-PCR (n = 3). Internal control, α-Tubulin. (O) The Protein expression of tight junction factors, ZO-1, VE-Cadherin, Claudin 5, and E-Cadherin, by Western blot. (P) The normalized protein expressions calculated by using ImageJ software (n = 3). Internal control, β-actin. (Q) The distribution of tight junction proteins, ZO-1, endothelium-specific markers (VE-Cadherin and Claudin 5), and epithelium-specific marker (E-Cadherin), by immunofluorescent staining in lung tissues. Images were magnified at 100 × . Scale bar, 100 μm *$P < 0.05$ vs Control. #$P < 0.05$ vs Model. †$P < 0.05$.

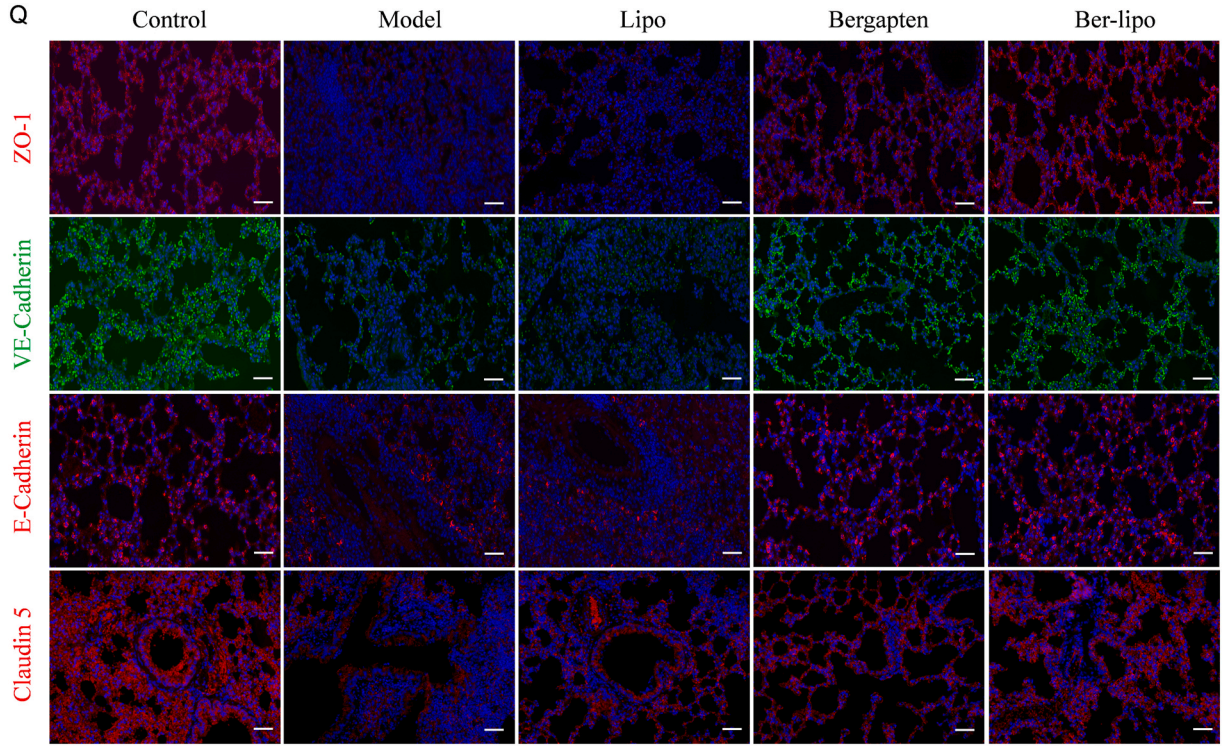

Fig. 5. (*continued*).

including ALI, was significantly relieved by Ber-lipo, implying a gradual recovery of ALI (Fig. 5D). The elevated lung index was also significantly reversed by Ber-lipo treatment, indicating a reduction of LPS-induced lung edema in ALI mice (Fig. 5E).

Moreover, the total protein concentration and total cell number in the BALF of mice were increased in the model group and relieved by inhalation of the drugs, suggesting that Ber-lipo mitigates LPS-induced damage to lung barrier (Fig. 5F & G). Lung function indices, PenH, TV/weight, and EF50, were measured using a noninvasive whole-body plethysmography method and showed a restoration of pulmonary function following treatment with Ber-lipo (Fig. 5H–J).

Furthermore, since lung barrier damage is associated with lung edema, lung inflammation, or lung injury displayed in ALI models [46, 47], Ber-lipo's effects on protecting lung endothelial-epithelial integrity were assessed in ALI mice. The expression patterns of endothelial barrier markers (Claudin5 and VE-Cadherin), epithelial barrier marker (E-Cadherin), and ZO-1 in lung tissues were analyzed using qRT-PCR, Western blot, and immunofluorescent staining. As shown in Fig. 5K-P, the mRNA and protein expressions of these markers were significantly reduced in the model group compared to the control, and this reduction was reversed in the drug treatment groups. Immunofluorescent staining also revealed a rescue of the declined expressions of ZO-1, VE-Cadherin, E-Cadherin, and Claudin 5 following treatment with Ber-lipo, indicating the recovery of lung barrier integrity (Fig. 5Q). In addition, in RNA sequencing (RNA-seq) analysis of lung tissues, cluster analysis of epithelium- and endothelium-related factors were conducted and further validated the protective effects of Ber-lipo on the lung barrier and relief of lung injury in ALI models (Fig. S7).

In summary, Ber-lipo ameliorated LPS-induced murine ALI, including relief of body weight loss, reduction of total protein and cell number in BALF, improvement of pulmonary function, attenuation of lung injury, inhibitory effects on lung inflammation, and maintenance of lung epithelial-endothelial integrity. These results indicate the potential therapeutic benefits of Ber-lipo in the treatment of ALI.

2.6. *Ber-lipo's effects on maintaining balance of macrophage polarization in vivo*

To validate Ber-lipo's effects on maintaining the homeostasis of M1/M2 macrophage polarization *in vivo*, we performed immunofluorescent staining, Western blot, and qRT-PCR to analyze the expression patterns of M1 and M2 phenotypic markers or cytokines released by them in lung tissues.

Immunofluorescent staining results showed that proinflammatory M1 markers, CD86 and iNOS, increased notably in the LPS-induced ALI model and then declined following treatments with bergapten and Ber-lipo, whereas anti-inflammatory M2 markers, CD206 and CD163, exhibited the opposite pattern (Fig. 6A). Western blot analysis displayed that CD86 protein was downregulated and CD163 protein significantly elevated by inhalation of the drugs, with Ber-lipo showing greater efficacy compared to bergapten (Fig. 6B-D).

Transcriptional expressions of M1-associated CD86 and iNOS were downregulated in the bergapten and Ber-lipo treatment groups compared to the model, while M2-associated CD206 and CD163 mRNA changed in the opposite manner (Fig. 6E-H). Additionally, the mRNA expressions of M1-released inflammatory factors (TNF-α, IL-6, and IL-1β) and M2-released anti-inflammatory cytokines (CCL22 and CCL24) were consistent with the changes of CD86/iNOS and CD206/CD163, respectively, indicating the transition from a proinflammatory state to an anti-inflammatory state in the pulmonary microenvironment (Fig. 6I-M).

In conclusion, Ber-lipo inhibited lung inflammation by resolving the

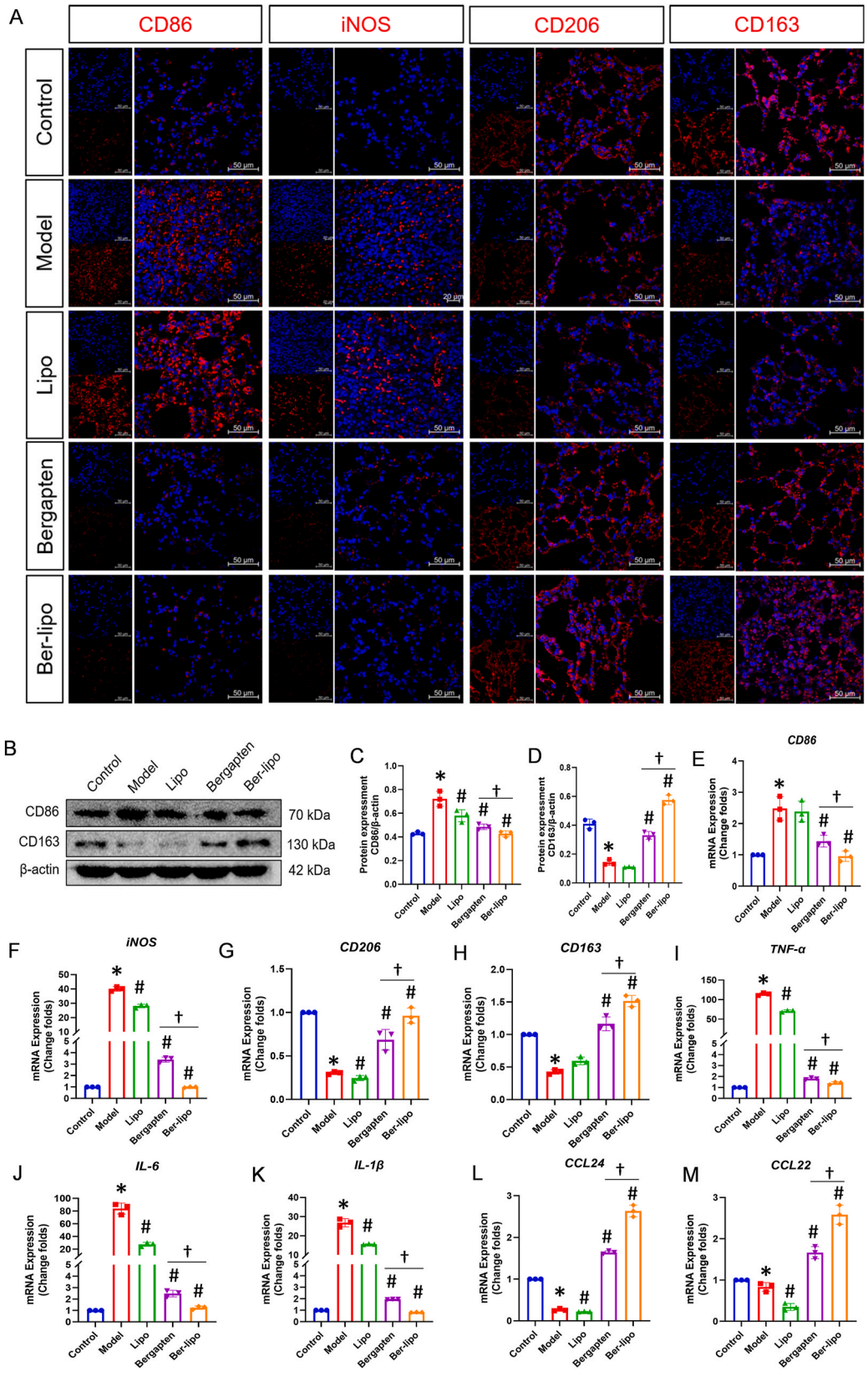

Fig. 6. Ber-lipo maintained balance between M1 and M2 macrophage polarization in lungs of ALI mice. (A) The expression patterns and distributions of M1 (CD86 and iNOS) and M2 (CD163 and CD206) markers by immunofluorescent staining. Images were taken under 40 × oil immersion lens of confocal macroscope. Scale bar, 50 μm. (B) Protein bands of CD86 (M1) and CD163 (M2) by Western blot. (C, D) Statistical analysis of proteins calculated by imageJ (n = 3). Internal control, β-actin. (E–M) The normalized transcriptional expressions of M1-associated genes (CD86, iNOS, TNF-α, IL-6, and IL-1β) and M2-associated ones (CD163, CD206, CCL22, and CCL24) by qRT-PCR (n = 3). Internal control, α-Tubulin. *$P < 0.05$ vs Control. #$P < 0.05$ vs Model. †$P < 0.05$.

imbalance between M1 and M2 macrophage polarization, which is crucial for the amelioration of lung injury. These findings support the potential therapeutic benefits of Ber-lipo in regulating macrophage polarization and alleviating lung inflammation in ALI.

2.7. Overall therapeutic effects of ber-lipo on ALI by RNA-seq in vivo

As described above, Ber-lipo exhibited satisfactory effects on treating ALI by regulating macrophage polarization, inhibiting inflammation, and protecting lung epithelial-endothelial integrity *in vitro* and *in vivo*. To further clarify Ber-lipo's overall therapeutic effects, transcriptional profiles of lung tissues were established using RNA-seq analysis.

The differentially expressed genes (DEGs) between the ALI model and control (Fig. S2), Lipo and control (Fig. S3), model and bergapten (Fig. S4), and model and Ber-lipo (Fig. S5) groups were intersected in a Venn diagram, revealing 2103 shared DEGs (Fig. 7A). All shared DEGs were clustered in a heatmap, showing that their mRNA levels in the bergapten/Ber-lipo treatment groups resembled those in the control and were opposite to those in the model and Lipo groups, suggesting rehabilitation of the inflamed lungs. Additionally, approximately three-quarters of DEGs were upregulated in the model but downregulated after the bergapten/Ber-lipo treatments, implying their close association with ALI phenotypes (Fig. 7B).

The upregulated DEGs in the model were subjected to disease, GO, KEGG, and reactome analyses, revealing enrichment in multiple inflammatory lung diseases (Fig. 7C), immune- and inflammation-related GO terms (Fig. 7D), and proinflammatory KEGG pathways (Fig. 7E) and reactomes (Fig. 7F), consistent with the experimental results. Furthermore, the downregulated DEGs in the model were found to be related to thalassemia and hypertensive diseases (Fig. 7G), suggesting that bergapten and Ber-lipo might not be suitable for patients with these diseases.

Cluster analysis of M1 and M2 phenotype-associated transcripts in a heatmap showed that inducible factors and markers of M1 were upregulated in the model and downregulated after bergapten and Ber-lipo treatments, while inducible factors and markers of M2 were upregulated in the bergapten/Ber-lipo treatment groups and downregulated in the model (Fig. 7H). Additionally, cluster analysis of key members in the TLR-MyD88-NF-κB signaling pathway [48,49] revealed that all of them were upregulated in the model/Lipo but downregulated in the other three groups (Fig. 7I), implying that Ber-lipo inhibits the activation of this pathway.

To validate whether Ber-lipo offers advantages over bergapten alone, a further analysis of the DEGs between bergapten and Ber-lipo treatments was conducted. As shown in Fig. S6A–6B, a smaller subset of DEGs were identified compared to those between model and Ber-lipo groups. The DEGs that were upregulated following bergapten treatment showed significant enrichment in multiple proinflammatory GO terms, signaling pathways, and reactomes (Fig. S6C–6E). In contrast, the downregulated DEGs were largely unrelate to proinflammatory terms (Fig. S6F-H), supporting that Ber-lipo possesses advantages over free bergapten in terms of anti-inflammatory properties.

Proinflammatory microenvironment is essential for inflammatory disease progression and subsequent organic injury. In general, disease with similar pathophysiological microenvironments may respond to similar therapeutic strategies. Like ALI, ischemic stroke also accompanies with uncontrolled inflammation, excess ROS, injured endothelial barrier, and macrophage activation [50,51]. As aforedescribed, Ber-lipo has demonstrated promising effects in attenuating these pathological factors, implying its potential for treating ischemic stroke. Additionally, Zhang et al. developed a pH/glutathione dual-responsive poly (amino acid) nanogel (NG/EDA) to target injury foci in brain to treat ischemic stroke, thereby avoiding drug leakage and potential damage to heathy tissues [50,51]. Thus, enhancing Ber-lipo's responsiveness to pathological environment may further boost its bioavailability and mitigate toxicity, thereby improving its therapeutic efficacy for inflammatory diseases beyond ALI such as ischemic stroke.

In conclusion, Ber-lipo demonstrated potential therapeutic effects on various inflammatory diseases, including ALI, by downregulating multiple proinflammatory signaling pathways and maintaining the balance between M1 and M2 polarization. The effects of Ber-lipo were found to be superior to those of bergapten for ALI treatment, consistent with the experimental results.

2.8. Mechanisms of ber-lipo ameliorating ALI

To further elucidate the mechanisms by which Ber-lipo treated ALI, we investigated the activation of the classical proinflammatory TLR4/MyD88/NF-κB signaling pathway in ALI progression. First, an in silico molecular docking analysis was performed to explore the potential interaction between bergapten and the key members in this pathway. The analysis revealed strong binding activities between bergapten and TLR4 (LPS receptor), MyD88, IκBα, and NF-κB p65(Fig. 8A).

Next, Western blot analysis was conducted for further validation in lung tissues. The protein expression of TLR4, MyD88, as well as the phosphorylation of IκBα and p65 were upregulated in the ALI model group compared to the control; however, Ber-lipo treatment (significantly better than free bergapten) reversed these upregulated proteins, indicating inhibition of the activation of the TLR4/MyD88/NF-κB signaling axis (Fig. 8B & C). Additionally, immunofluorescent staining was performed to observe the distribution of NF-κB p65 in the nuclei of RAW264.7 cells exposed to LPS. It was found that NF-κB p65 nuclear translocation occurred in nearly 100% of cells after LPS treatment for 24 h, but bergapten/Ber-lipo treatments partially inhibited this phenomenon, demonstrating the modulation of the NF-κB signaling pathway (Fig. 8D).

It was revealed that Ber-lipo effectively suppressed the activation of the TLR4/MyD88/NF-κB pathway, which may be a critical mechanism by which Ber-lipo exerts its therapeutic effects on ALI. This mechanism involves the modulation of macrophage polarization and the repair of the lung barrier. As reported, the activation of TLR4 signaling axis [52] and the dysregulation of M1/M2 macrophage polarization [53] are both factors that can exacerbate ALI and lung barrier damage, which further supported our findings.

LPS is a common pathogenic factor from gram-negative bacteria and is often used to induce inflammatory diseases such as ALI [54,55]. In ALI progression, LPS is specifically recognized by TLR4, which then recruits MyD88 to promote the phosphorylation and degradation of IκBα, triggering NF-κB p65 nuclear translocation to initiate downstream inflammatory responses, such as the release of TNF-α, IL-1β, and IL-6. Ber-lipo was found to negatively regulate the activation of the TLR4/MyD88/NF-κB pathway (Fig. 9), revealing the mechanism by which Ber-lipo attenuates ALI. Furthermore, since this pathway is related to many other epidemic inflammatory diseases such as lung fibrosis [56], it is speculated that Ber-lipo may also have beneficial effects on these conditions, which warrants further investigation in the future.

3. Conclusion

In this study, a novel inhalable and lung-targeted lipid-nanomedicine (Ber-lipo) was successfully developed for enhanced ALI therapy. Ber-lipo showed clear advantages over free bergapten in terms of solubility in water, biodistribution, and efficacy in targeted therapy against ALI. *In vitro*, Ber-lipo helped balance M1/M2 macrophage polarization, inhibited inflammation, and protected epithelial–endothelial integrity. *In vivo*, Ber-lipo significantly ameliorated ALI phenotypes, including relief of lung edema and inflammation, improvement of pulmonary function, recovery of lung lesions, and repair of lung barrier.

In the pulmonary microenvironment, Ber-lipo reprogrammed M1/M2 macrophage polarization to an anti-inflammatory state. At the transcriptome level, Ber-lipo exhibited potential in treating

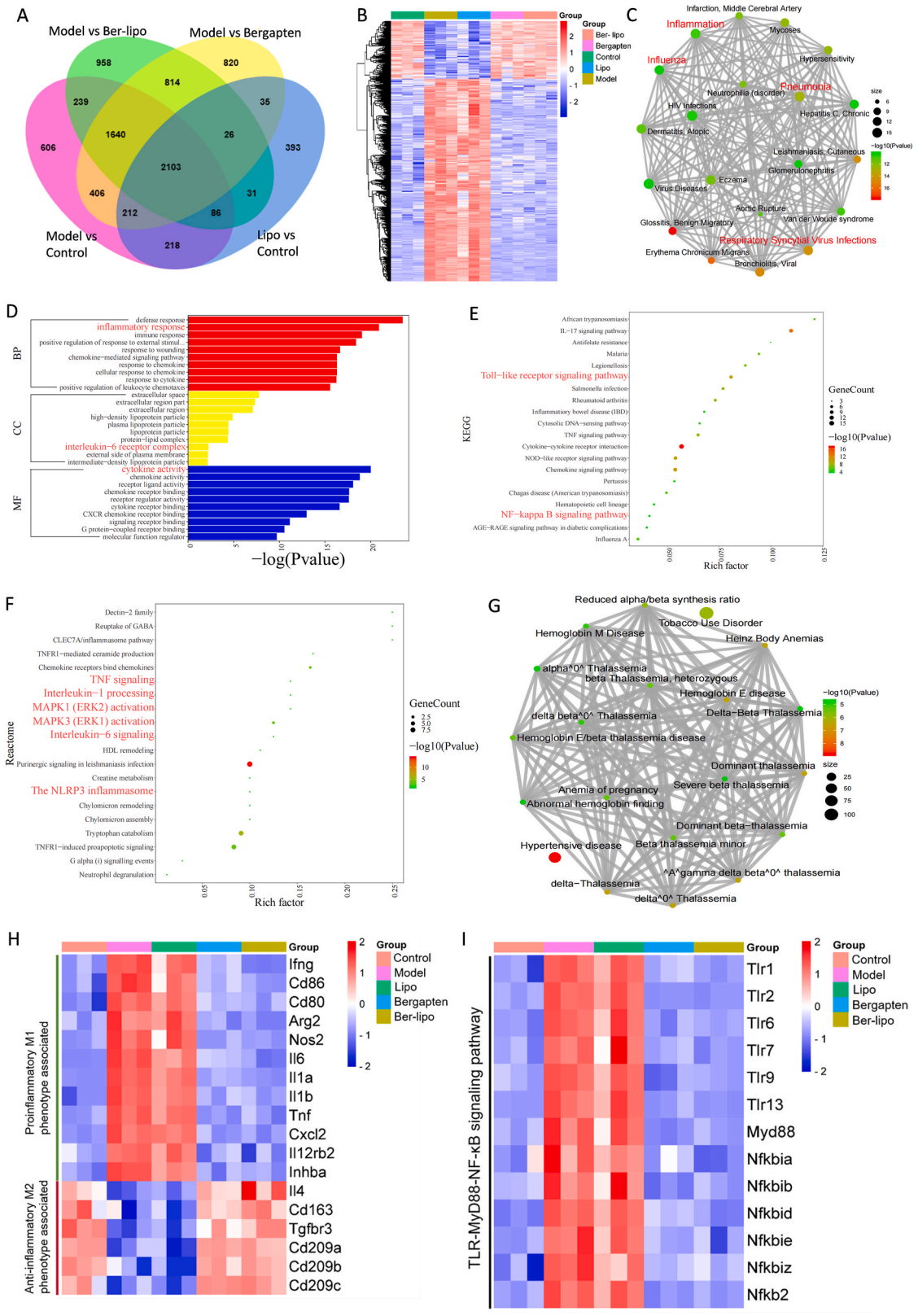

Fig. 7. Ber-lipo's overall effects on treating ALI by RNA-seq analysis of lung tissues. (A) The DEGs from different comparison groups intersected in a venn diagram, including model vs. control, Lipo vs. control, model vs. Ber-lipo, and model vs. bergapten. (B) Cluster analysis of a total of 2103 intersected DEGs in A by heatmap. The upregulated DEGs in the model subjected to (C) disease enrichment analysis in a net plot, (D) GO analysis in a bar plot, (E) KEGG analysis in a bubble diagram, and (F) reactome analysis also in a bubble diagram. Inflammatory terms were marked in red. (G) The upregulated DEGs in the bergapten and Ber-lipo groups analyzed for disease enrichment analysis. (H) Cluster analysis of M1 and M2 macrophage-associated DEGs among all groups. (I) Cluster analysis of the key DEGs in the TLR-MyD88-NF-κB signaling pathway.

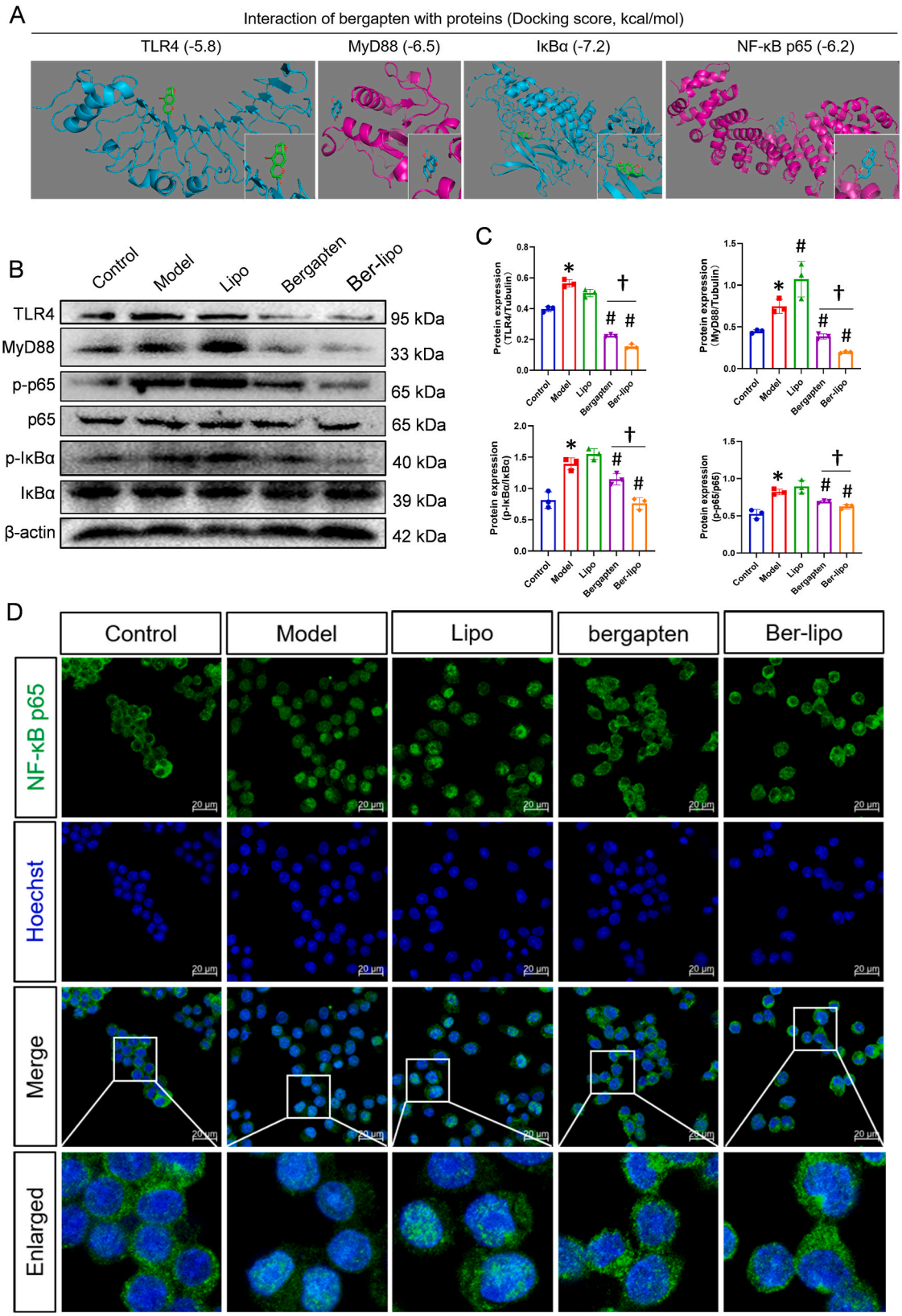

Fig. 8. Ber-lipo inhibited the activation of TLR4/MyD88/NF-κB signaling pathway. (A) The binding activity of bergapten to TLR4, MyD88, IκBα, and NF-κB p65 proteins showed by an in silico molecular docking analysis. (B) The protein expressions of key members in the TLR4/MyD88/NF-κB pathway by Western blot, including TLR4, MyD88, the phosphorylated (p-p65) and basal NF-κB p65, p-IκBα, and IκBα. (C) The normalized expression of the proteins calculated by ImageJ software. (D) NF-κB p65 nuclear translocation by immunofluorescent staining and imaged by 40 × oil immersion lens of confocal microscope. Scale bar, 20 μm *$P <$ 0.05 vs Control. #$P < 0.05$ vs Model. †$P < 0.05$.

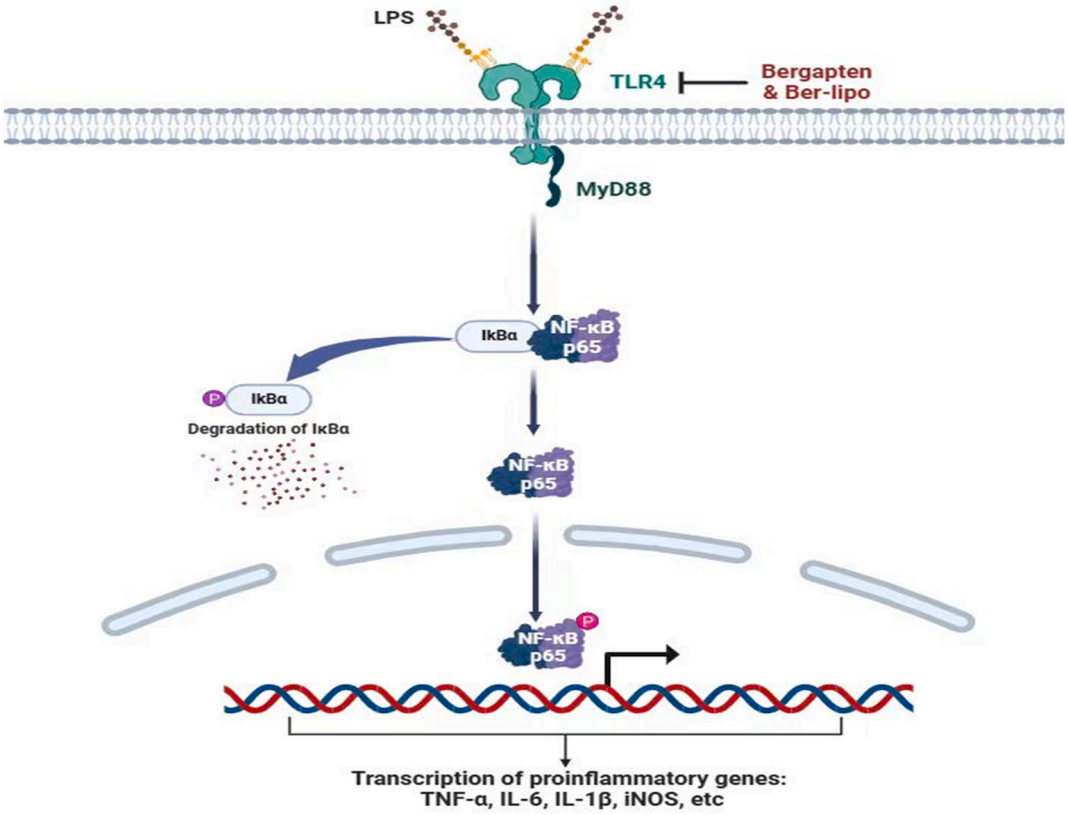

Fig. 9. The mechanism of Ber-lipo inhibiting the activation of TLR4/MyD88/NF-κB signaling pathway to restrain proinflammatory state. In brief, Ber-lipo inhibited TLR4 (LPS receptor) expression, then reduced the recruitment of MyD88, and further suppressed the IκBα activation, thereby hijacking NF-κB p65 nuclear translocation to mitigate inflammatory response.

inflammatory lung diseases such as pneumonia by inhibiting multiple proinflammatory signals and modulating M1/M2 macrophage-associated genes' expressions. Mechanically, molecular docking and Western blot validated that Ber-lipo suppressed the activation of TLR4/MyD88/NF-κB signaling axis responsible for ALI progression.

Considering the observed properties and effects of Ber-lipo in inhibiting inflammation, repairing epithelial-endothelial barriers, and orchestrating macrophage polarization, it is imperative to delve deeper into its significance and broader implications. Notably, similar pathophysiological microenvironments exist in a variety diseases, such as sepsis, viral pneumonia, and ischemic stroke. The potential therapeutic effects of Ber-lipo in treating these disorders deserve in-depth investigation. In addition, Lipo containing pulmonary surfactants, such as DPPC, demonstrates significant advantages on reducing drug toxicity and enhancing lung-targeting capability. Thus, this drug delivery strategy offers promising opportunities to overcome the obstacles associated with numerous natural compounds, such as toxicity, water insolubility, or poor lung-targeting, thereby potentially facilitating their clinical practice.

Taken together, our findings demonstrate, for the first time, that new Ber-lipo achieves satisfactory effects in treating ALI by maintaining the homeostasis of macrophage polarization via the inactivation of the TLR4/MyD88/NF-κB signaling pathway. This study provides an effective and promising strategy for the treatment of ALI/ARDS in the clinic.

Ethics approval and consent to participate

All animal assays were conducted in accordance with the guidelines of the IACUC of Guangzhou University of Chinese Medicine and approved by the Experimental Animal Research Center of the Second Affiliated Hospital of Guangzhou University of Chinese Medicine (Permit No. 2023017).

Data availability statement

The data that support the findings of this study are available on request from the corresponding author.

CRediT authorship contribution statement

Ran Liao: Writing – review & editing, Writing – original draft, Validation, Methodology, Investigation, Formal analysis, Data curation. **Zhi-Chao Sun:** Writing – review & editing, Validation, Software, Methodology, Investigation, Funding acquisition, Formal analysis. **Liying Wang:** Writing – review & editing, Visualization, Validation, Methodology, Investigation, Formal analysis. **Caihong Xian:** Visualization, Validation, Methodology. **Ran Lin:** Visualization, Resources, Methodology. **Guifeng Zhuo:** Visualization, Resources, Methodology. **Haiyan Wang:** Visualization, Methodology. **Yifei Fang:** Methodology, Formal analysis. **Yuntao Liu:** Validation, Supervision, Project administration, Data curation. **Rongyuan Yang:** Supervision, Project administration, Methodology, Conceptualization. **Jun Wu:** Writing – review & editing, Supervision, Project administration, Funding acquisition, Formal analysis, Data curation, Conceptualization. **Zhongde Zhang:** Writing – review & editing, Visualization, Supervision, Project administration, Methodology, Funding acquisition, Data curation, Conceptualization.

Declaration of competing interest

The authors declare no conflict of interest.

Acknowledgements

This work was supported by grants from the National Natural Science Foundation of China (52173150, 82374392), Guangdong Provincial Key Laboratory of Research on Emergency in TCM (2023B1212060062), Innovation Team and Talents Cultivation Program of National Administration of Traditional Chinese Medicine (ZYYCXTD-D-202203), Guangzhou Key Laboratory of Integrated Traditional Chinese and Western Medicine for the Prevention and Treatment of Emerging infectious diseases (202201020382), Guangdong Provincial Bureau of Chinese Medicine (20241121), Postdoctoral Program of Guangdong Provincial Hospital of Chinese Medicine (B1), the Guangzhou Science and Technology Program City-University Joint Funding Project (2024A03J0604).

Appendix A. Supplementary data

Supplementary data to this article can be found online at https://doi.org/10.1016/j.bioactmat.2024.09.020.

References

[1] E. Fan, D. Brodie, A.S. Slutsky, Acute respiratory distress syndrome: advances in diagnosis and treatment, JAMA 319 (7) (2018) 698–710.
[2] L. Xia, C. Zhang, N. Lv, et al., AdMSC-derived exosomes alleviate acute lung injury via transferring mitochondrial component to improve homeostasis of alveolar macrophages, Theranostics 12 (6) (2022) 2928–2947.
[3] M.E. Long, R.K. Mallampalli, J.C. Horowitz, Pathogenesis of pneumonia and acute lung injury, Clin Sci (Lond). 136 (10) (2022) 747–769.
[4] D. Marzioni, R. Mazzucchelli, S. Fantone, et al., NRF2 modulation in TRAMP mice: an *in vivo* model of prostate cancer, Mol. Biol. Rep. 50 (1) (2023) 873–881.
[5] S. Ghareghomi, M. Habibi-Rezaei, M. Arese, et al., Nrf2 modulation in breast cancer, Biomedicines 10 (10) (2022) 2668.
[6] C.S. Calfee, K.L. Delucchi, P. Sinha, et al., Acute respiratory distress syndrome subphenotypes and differential response to simvastatin: secondary analysis of a randomised controlled trial, Lancet Respir. Med. 6 (9) (2018) 691–698.
[7] M.A. Matthay, R.L. Zemans, G.A. Zimmerman, et al., Acute respiratory distress syndrome, Nat. Rev. Dis. Prim. 5 (1) (2019) 18.
[8] R.M. Sweeney, D.F. McAuley, Acute respiratory distress syndrome, Lancet 388 (10058) (2016) 2416–2430.
[9] Z. Wang, J. Li, J. Cho, et al., Prevention of vascular inflammation by nanoparticle targeting of adherent neutrophils, Nat. Nanotechnol. 9 (3) (2014) 204–210.
[10] C. Liu, K. Xiao, L. Xie, Advances in mesenchymal stromal cell therapy for acute lung injury/acute respiratory distress syndrome, Front. Cell Dev. Biol. 10 (2022) 951764.
[11] Y.Q. He, C.C. Zhou, L.Y. Yu, et al., Natural product derived phytochemicals in managing acute lung injury by multiple mechanisms, Pharmacol. Res. 163 (2021) 105224.
[12] J. Guo, K. Su, L. Wang, et al., Poly(p-coumaric acid) nanoparticles alleviate temporomandibular joint osteoarthritis by inhibiting chondrocyte ferroptosis, Bioact. Mater. 40 (2024) 212–226.
[13] F. De Amicis, S. Aquila, C. Morelli, et al., Bergapten drives autophagy through the up-regulation of PTEN expression in breast cancer cells, Mol. Cancer 14 (2015) 130.
[14] E.A. Adakudugu, D.D. Obiri, E.O. Ameyaw, et al., Bergapten modulates ovalbumin-induced asthma, Sci African 8 (2020) e00457.
[15] D.B. Aidoo, D.D. Obiri, N. Osafo, et al., Allergic airway-induced hypersensitivity is attenuated by bergapten in murine models of inflammation, Adv Pharmacol Sci 2019 (2019) 6097349.
[16] C.Y. Zhang, J. Gao, Z. Wang, Bioresponsive nanoparticles targeted to infectious microenvironments for sepsis management, Adv Mater 30 (43) (2018) e1803618.
[17] J. Liu, X. You, L. Wang, et al., ROS-responsive and self-tumor curing methionine polymer library based nanoparticles with self-accelerated drug release and hydrophobicity/hydrophilicity switching capability for enhanced cancer therapy, Small 20 (2024) 2401438.
[18] S. Bian, H. Cai, Y. Cui, et al., Nanomedicine-based therapeutics to combat acute lung injury, Int J Nanomedicine 16 (2021) 2247–2269.
[19] H. Shi, X. Zhao, J. Gao, et al., Acid-resistant ROS-responsive hyperbranched polythioether micelles for ulcerative colitis therapy, Chin. Chem. Lett. 31 (2020) 3102–3106.
[20] R. Su, Y. Zhang, J. Zhang, et al., Nanomedicine to advance the treatment of bacteria-induced acute lung injury, J. Mater. Chem. B 9 (44) (2021) 9100–9115.
[21] Q. Qiao, X. Liu, T. Yang, et al., Nanomedicine for acute respiratory distress syndrome: the latest application, targeting strategy, and rational design, Acta Pharm. Sin. B 11 (10) (2021) 3060–3091.
[22] Yifei Fang, Tianqi Nie, Guangze Li, et al., Multifunctional antibiotic hydrogel doped with antioxidative lycopene-based liposome for accelerative diabetic wound healing, Chem Eng J 480 (2024) 147930.
[23] Y. Yu, S. Li, Y. Yao, et al., Increasing stiffness promotes pulmonary retention of ligand-directed dexamethasone-loaded nanoparticle for enhanced acute lung inflammation therapy, Bioact. Mater. 20 (2022) 539–547.
[24] B.S. Schuster, A.J. Kim, J.C. Kays, et al., Overcoming the cystic fibrosis sputum barrier to leading adeno-associated virus gene therapy vectors, Mol. Ther. 22 (8) (2014) 1484–1493.
[25] Q. Fan, Y.E. Wang, X. Zhao, et al., Adverse biophysical effects of hydroxyapatite nanoparticles on natural pulmonary surfactant, ACS Nano 5 (8) (2011) 6410–6416.
[26] X. Chen, J. Tang, W. Shuai, et al., Macrophage polarization and its role in the pathogenesis of acute lung injury/acute respiratory distress syndrome, Inflamm. Res. 69 (9) (2020) 883–895.
[27] B. Robertson, Lung surfactant for replacement therapy, Clin. Physiol. 3 (2) (1983) 97–110.
[28] S. Arber Raviv, M. Alyan, E. Egorov, et al., Lung targeted liposomes for treating ARDS, J. Contr. Release 346 (2022) 421–433.
[29] H. Chen, Z. Liu, B. Wei, et al., Redox responsive nanoparticle encapsulating black phosphorus quantum dots for cancer theranostics, Bioact. Mater. 6 (3) (2020) 655–665.
[30] S. Walker, S. Busatto, A. Pham, et al., Extracellular vesicle-based drug delivery systems for cancer treatment, Theranostics 9 (26) (2019) 8001–8017.
[31] C. Liu, Y. Liu, L. Xi, et al., Interactions of inhaled liposome with macrophages and neutrophils determine particle biofate and anti-inflammatory effect in acute lung inflammation, ACS Appl. Mater. Interfaces 15 (1) (2023) 479–493.
[32] R. Tenchov, R. Bird, A.E. Curtze, et al., Lipid Nanoparticles—From liposomes to mRNA vaccine delivery, a landscape of research diversity and advancement, ACS Nano 15 (11) (2021) 16982–17015.
[33] S.T. LoPresti, M.L. Arral, N. Chaudhary, et al., The replacement of helper lipids with charged alternatives in lipid nanoparticles facilitates targeted mRNA delivery to the spleen and lungs, J. Contr. Release 345 (2022) 819–831.
[34] L. Xue, A.G. Hamilton, G. Zhao, et al., High-throughput barcoding of nanoparticles identifies cationic, degradable lipid-like materials for mRNA delivery to the lungs in female preclinical models, Nat. Commun. 15 (1) (2024) 1884.
[35] J. Yang, J. Ding, Nanoantidotes: a detoxification system more applicable to clinical practice, BME Front. 2023 (2023) 20.
[36] J. Yang, T. Su, H. Zou, et al., Spatiotemporally targeted polypeptide nanoantidotes improve chemotherapy tolerance of cisplatin, Angew Chem. Int. Ed. Engl. 61 (47) (2022) e202211136.
[37] G.F. Gerber, X. Yuan, J. Yu, et al., COVID-19 vaccines induce severe hemolysis in paroxysmal nocturnal hemoglobinuria, Blood 137 (26) (2021) 3670–3673.
[38] Z. Wang, Z. Wang, The role of macrophages polarization in sepsis-induced acute lung injury, Front. Immunol. 14 (2023) 1209438.
[39] Q. Qiao, X. Liu, K. Cui, et al., Hybrid biomimetic nanovesicles to drive high lung biodistribution and prevent cytokine storm for ARDS treatment, ACS Nano 16 (9) (2022) 15124–15140.
[40] Z. Hao, L. Ren, Z. Zhang, et al., A multifunctional neuromodulation platform utilizing Schwann cell-derived exosomes orchestrates bone microenvironment via immunomodulation, angiogenesis and osteogenesis, Bioact. Mater. 23 (2022) 206–222.
[41] R.S. Patil, M.E. Maloney, R. Lucas, et al., Zinc-dependent histone deacetylases in lung endothelial pathobiology, Biomolecules 14 (2) (2024) 140.
[42] J. Jiang, K. Huang, S. Xu, et al., Targeting NOX4 Alleviates Sepsis-Induced Acute Lung Injury via Attenuation of Redox-Sensitive Activation of CaMKII/ERK1/2/MLCK and Endothelial Cell Barrier Dysfunction, vol. 36, 2020 101638.
[43] A. Huertas, C. Guignabert, J.A. Barberà, et al., Pulmonary vascular endothelium: the orchestra conductor in respiratory diseases: highlights from basic research to therapy, Eur. Respir. J. 51 (4) (2018) 1700745.
[44] L. Shao, D. Meng, F. Yang, et al., Irisin-mediated protective effect on LPS-induced acute lung injury via suppressing inflammation and apoptosis of alveolar epithelial cells, Biochem. Biophys. Res. Commun. 487 (2) (2017) 194–200.
[45] M. Fang, W.H. Zhong, W.L. Song, et al., Ulinastatin ameliorates pulmonary capillary endothelial permeability induced by sepsis through protection of tight junctions via inhibition of TNF-α and related pathways, Front. Pharmacol. 9 (2018) 823.
[46] S. Herold, N.M. Gabrielli, I. Vadász, Novel concepts of acute lung injury and alveolar-capillary barrier dysfunction, Am. J. Physiol. Lung Cell Mol. Physiol. 305 (10) (2013) L665–L681.
[47] J. Bhattacharya, M.A. Matthay, Regulation and repair of the alveolar-capillary barrier in acute lung injury, Annu. Rev. Physiol. 75 (2013) 593–615.
[48] H. Zhang, X. You, X. Wang, et al., Delivery of mRNA vaccine with a lipid-like material potentiates antitumor efficacy through Toll-like receptor 4 signaling, Proc Natl Acad Sci U S A. 118 (6) (2021) e2005191118.
[49] A.Q. Ren, H.J. Wang, H.Y. Zhu, et al., Glycoproteins from rabdosia japonica var. glaucocalyx regulate macrophage polarization and alleviate lipopolysaccharide-induced acute lung injury in mice via TLR4/NF-κB pathway, Front. Pharmacol. 12 (2021) 693298.
[50] Y. Zhang, Z. Zou, S. Liu, et al., Edaravone-loaded poly(amino acid) nanogel inhibits ferroptosis for neuroprotection in cerebral ischemia injury, Asian J. Pharm. Sci. 19 (2) (2024) 100886.
[51] Y. Zhang, H. Liu, J. Ding, Brain-targeted drug delivery platforms for ischemic stroke therapy, BME Front 5 (2024) 55.
[52] Y. Wu, X. Yu, Y. Wang, et al., Ruscogenin alleviates LPS-triggered pulmonary endothelial barrier dysfunction through targeting NMMHC IIA to modulate TLR4 signaling, Acta Pharm. Sin. B 12 (3) (2022) 1198–1212.
[53] Z. Wang, Z. Wang, The role of macrophages polarization in sepsis induced acute lung injury, Front. Immunol. 14 (2023) 1209438.

[54] H.F. Håkansson, A. Smailagic, C. Brunmark, et al., Altered lung function relates to inflammation in an acute LPS mouse model, Pulm. Pharmacol. Ther. 25 (5) (2012) 399–406.
[55] X. Ma, X. Li, Q. Di, et al., Natural molecule Munronoid I attenuates LPS-induced acute lung injury by promoting the K48-linked ubiquitination and degradation of TAK1, Biomed. Pharmacother. 138 (2021) 111543.
[56] S. Li, G. Liu, M. Gu, et al., A novel therapeutic approach for IPF: based on the "Autophagy - apoptosis" balance regulation of Zukamu Granules in alveolar macrophages, J. Ethnopharmacol. 297 (2022) 115568.